



ATLAS NOTE

ATLAS-CONF-2011-051

March 30, 2011



Data-driven estimation of the background to charged Higgs boson searches using hadronically-decaying τ final states in ATLAS

The ATLAS Collaboration

Abstract

The experimental observation of charged Higgs bosons, H^\pm , which are theoretically predicted by many non-minimal Higgs scenarios, would indicate new physics beyond the Standard Model. In the Minimal Supersymmetric Standard Model, for example, the dominant production mode at the LHC for these Higgs bosons, when $m_{H^+} < m_t$, takes place in $t\bar{t}$ events via the top-quark decay $t \rightarrow H^+ b$ with $H^+ \rightarrow \tau \nu$ dominating for most values of $\tan\beta$. Two channels with a hadronically decaying τ coming from the charged Higgs boson are studied. The delivery of the first 37 pb^{-1} of $\sqrt{s} = 7 \text{ TeV}$ collision data allows many significant backgrounds to be estimated with data-driven methods, which represent the primary focus of this note and a crucial step towards ATLAS searches for the charged Higgs boson.

1 Introduction

The charged Higgs boson is predicted by many non-minimal Higgs scenarios such as models containing Higgs triplets and 2-Higgs-Doublet Models (2HDM) [1, 2, 3]. The experimental observation of charged Higgs bosons¹, H^\pm , would indicate new physics beyond the Standard Model. The first experimental evidence for the Minimal Supersymmetric Standard Model (MSSM) might very well come from their discovery at the Large Hadron Collider (LHC), if the model is realized in nature, and supersymmetric particles are heavy enough to evade detection [4]. The analyses in this note only consider the 2HDM, more specifically the Type II-2HDM, which describes the Higgs sector of the MSSM.

The dominant production mode at the LHC for these Higgs bosons for the case that the charged Higgs boson mass (m_{H^\pm}) is smaller than the top-quark mass (m_t) are $t\bar{t}$ events via the top-quark decay $t \rightarrow H^+ b$ with $H^+ \rightarrow \tau\nu$ (see Figure 1). The $H^+ \rightarrow \tau\nu$ decay mode dominates if the ratio of the vacuum expectation values of the two Higgs doublets ($\tan\beta$) is larger than 3. Production in the τ +jets channel occurs when one of the two top quarks decays to $Wb \rightarrow jjb$. Similarly, signal events considered by the τ +lepton channel come about when one of the top quarks decays to $Wb \rightarrow l\nu b$ ($l = e, \mu$ or leptonically decaying τ). Both channels are studied here, but this note only considers a hadronically-decaying τ coming from the charged Higgs boson.

The background processes that enter these searches include the production of $t\bar{t}$, single top-quark, W +jets, Z +jets, and QCD multi-jet events. The delivery of the first collision data with a centre-of-mass energy of $\sqrt{s} = 7$ TeV allows many significant backgrounds to be estimated in a data-driven way, a crucial step toward searches for these bosons in the near future using ATLAS datasets with larger integrated luminosity. The methods used for background estimation are based on embedding τ jets in events with muons, and on the measured probabilities for jets, electrons, and muons to be misidentified as τ jets. Finally, the QCD multi-jet background is estimated in the τ +jets analysis using a data-driven control sample. The studies are based on proton-proton collision data collected at the LHC at a centre-of-mass energy of $\sqrt{s} = 7$ TeV in 2010. Only data-taking runs where all detector systems were fully operational and stable beam conditions were fulfilled are used. The total investigated luminosity corresponds to up to 37 pb^{-1} and depends slightly on the trigger streams used.

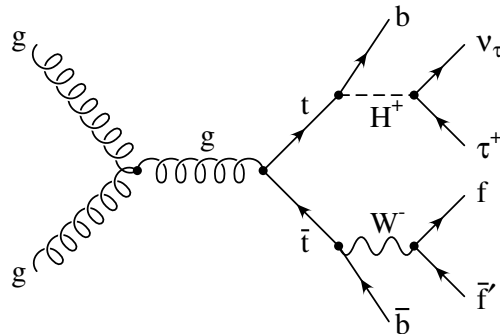


Figure 1: Leading-order Feynman diagram for the production of a charged Higgs boson through gluon fusion in $t\bar{t}$ decays.

2 Physics processes and cross sections

The Monte Carlo (MC) simulation of $t\bar{t}$ and single top-quark events from proton-proton collisions at $\sqrt{s} = 7$ TeV is done with MC@NLO [5] using HERWIG [6] for hadronization and JIMMY [7] for the

¹Hereafter the charged Higgs bosons will be denoted H^\pm , with the charge-conjugate processes implied.

underlying event. Overlap between $t\bar{t}$ and single top-quark final states is removed in these MC@NLO samples [8]. A $t\bar{t}$ production cross section of 164.6 pb [9] obtained from NLO+NNLL calculations [10] is used (both for Standard-Model-like $t\bar{t}$ and decays via H^+); the MC@NLO values are used for single top-quark production.

ALPGEN [11] is used for the generation of W and Z events with up to five additional partons, again together with HERWIG/JIMMY. The MLM matching scheme [12] is employed, with the jet p_T and ΔR cuts set to 20 GeV and 0.7, respectively. The ALPGEN cross sections are rescaled by a factor 1.20 (W) and 1.25 (Z) to match NNLO calculations [4]. The $b\bar{b}$ and H^+ events are generated with PYTHIA [13], using TAUOLA [14] for τ lepton decays and PHOTOS [15] for photon radiation off charged leptons. Events hadronized by PYTHIA use the ATLAS MinBias Tune 1 [16], while HERWIG/JIMMY samples use the ATLAS Underlying Event Tune 1 [17]. The simulated events and cross sections used are summarized in Table 1. The expected number of events is given by the production cross section times the integrated luminosity, which is 37 pb^{-1} for the lepton triggers, and 36 pb^{-1} for the hadronically-decaying- τ plus E_T^{miss} trigger. All events are passed through a detailed ATLAS detector simulation [18] using GEANT4 [19] and reconstructed by the same algorithms as the data.

Table 1: Simulated events used in this study. The W/Z +jets, $t\bar{t}$, as well as the s - and t -channel single top-quark events are only simulated for decays involving leptons (e , μ , or τ), and the cross section given includes this branching ratio. NLO+NNLL calculations are used for $t\bar{t}$, NLO for single top-quark, NNLO for W/Z +jets, and LO for $b\bar{b}$. The $b\bar{b}$ cross section is given for the phase space with at least one muon in the decay chain with $p_T > 15 \text{ GeV}$. The H^+ sample uses $m_{H^+} = 130 \text{ GeV}$ and $\tan\beta = 35$ as input.

Process	Generator	Cross section [pb]
$t\bar{t}$ with $\geq 1\ell$	MC@NLO	89.7
single top-quark (s , t , Wt channel)	MC@NLO	21.4, 1.41, 14.6
$W \rightarrow \ell\nu$ +jets	ALPGEN	$3.1 \cdot 10^4$
$Z \rightarrow \ell\ell$ +jets	ALPGEN	$3.2 \cdot 10^3$
$b\bar{b}$ with μ filter	PYTHIAB	$7.4 \cdot 10^4$
$t\bar{t} \rightarrow bH^\pm bW$ with $H^\pm \rightarrow \tau\nu$	PYTHIA	18.5

3 Object reconstruction

In this section, the common object reconstruction for the τ +jets and τ +lepton event selections are detailed. For data-driven background estimation methods based on fake rates, requirements on the tag objects are explained in the respective sections should they differ.

Event-level cleaning cuts For both the H^+ event selection and the data-driven background estimates several general-purpose event quality requirements [20] are always applied. To further reject non-collision backgrounds, only events with a reconstructed primary vertex with at least five associated tracks are considered.

Jets Jets are reconstructed with the anti- k_T algorithm [21, 22] with a size parameter value of 0.4, using three-dimensional topological clusters as input [23, 24]. The electromagnetic calibration of the ATLAS calorimeters is converted to the hadronic scale by a calibration scheme depending on p_T , η and the number of primary vertices in the event [25]. Jets are required to have $p_T > 20 \text{ GeV}$ and $|\eta| < 4.9$. While the standard ATLAS definition is $|\eta| < 4.5$, a looser pseudorapidity cut is used in this work.

τ jets For the reconstruction of hadronically-decaying τ s, anti- k_T jets in the calorimeter with $E_T > 10$ GeV are used as seeds. Electron and muon vetoes are applied at this stage, and $p_T > 20$ GeV, $|\eta| < 2.5$, and 1 or 3 associated tracks are required. Objects passing this selection are referred to as “ τ jet candidates”. Additionally, medium (tight) quality cuts on the τ log-likelihood identification are applied for 1-track (multi-track) τ jet candidates [26], to discriminate τ jets from jets not initiated by τ leptons.

b jets A secondary-vertex tagger with a nominal efficiency of about 50% is used to identify those jets containing b quarks among all jets passing the reconstruction discussed above [27].

Electrons Electrons are reconstructed by matching energy depositions in clusters of electromagnetic calorimeter cells to a track in the inner tracking detector [28]. The shower-shape information is used to increase the quality of the electron identification. Candidates are required to have $p_T > 20$ GeV (for lepton vetoes, this value is lowered to 10 GeV), and to be in the pseudorapidity ranges $0 < |\eta| < 1.37$ or $1.52 < |\eta| < 2.47$. Only isolated electrons are considered by requiring that the deposited energy in a calorimeter cone of $\Delta R < 0.2$ around the electron² is less than 4 GeV plus 2.3% of the electron E_T .

Muons Objects are considered as muon candidates if an inner detector track matches a track reconstructed in the muon spectrometer [29]. Candidates are required to have $p_T > 20$ GeV (for lepton vetoes, this value is lowered to 10 GeV) and $|\eta| < 2.5$. Only isolated muons are considered by requiring that in a cone of $\Delta R < 0.3$ around the muon, both the energy deposited in the calorimeters and the momentum of all inner detector tracks total less than 4 GeV. Additionally, an angular distance to any jet with $E_T > 20$ GeV of $\Delta R > 0.4$ is required.

Missing transverse energy, transverse energy sum The missing transverse energy, E_T^{miss} , is based on the energy deposited in the calorimeter and the momentum of tracks identified as associated to muons. The contribution of the calorimeter cells is calibrated differently depending on the object to which they are associated. For all jets, the same hadronic calibration scheme as for jet reconstruction is used while electrons are calibrated at the electromagnetic scale [30].

The transverse energy sum, ΣE_T , is defined as the sum of the transverse energy of all objects which have been reconstructed as detailed in this section, i.e., electrons, muons, τ jets, b -tagged jets, light jets, and E_T^{miss} .

The missing transverse energy significance, $E_T^{\text{miss}} / \sqrt{\Sigma E_T}$, is a complex quantity used to suppress QCD multi-jet events without losing a large number of signal events (simply increasing the E_T^{miss} requirement would be detrimental to the τ +jets analysis). As discussed in Reference [31], investigations have shown that this quantity is well-modeled for events with a large amount of true E_T^{miss} .

Overlap removal When candidates selected using the above criteria overlap within $\Delta R < 0.2$, this is resolved by calling the object a muon, electron, τ jet, or jet, in this order of priority.

3.1 Object-related systematic uncertainties

Uncertainties on the reconstruction and identification of leptons, τ jets and other jets, as well as the momentum or energy resolution/scale of these objects, comprise the dominant detector-related contributions to the systematic uncertainties. Additionally, uncertainties due to missing transverse energy reconstruction, the trigger, and measured luminosity are considered.

² $\Delta R = \sqrt{(\Delta\eta)^2 + (\Delta\phi)^2}$, where η is the pseudorapidity and ϕ the azimuthal angle.

In lieu of a sizeable sample of true τ jets collected from collision data, the systematic uncertainty for the $\tau+E_T^{\text{miss}}$ trigger is estimated from the differences between simulation and data observed for this trigger in QCD multi-jet events. This results in a conservative estimate as the comparison is done on QCD multi-jet events rather than true τ jets—where the systematic effect is expected to be smaller. The statistical uncertainty on the ratio of the simulation-to-data trigger efficiencies (which is compatible with 1), in a region of transverse energy that benefits from large statistics, is taken as the systematic uncertainty on the τ trigger efficiency (11%). For the E_T^{miss} trigger efficiency, the systematic uncertainty is taken as the largest simulation-to-data discrepancy observed for events with $E_T^{\text{miss}} > 50$ GeV (where the bulk of selected data lies) and is 5%. The τ and E_T^{miss} trigger uncertainties are combined under the assumption that they are uncorrelated.

The dominating experimental systematic uncertainties for the H^+ studies are summarized in Table 2. To assess the impact of most systematic sources on either the τ +jets or the τ +lepton channel, the selection cuts for each analysis are applied after shifting a particular parameter to its upper and lower extrema. The luminosity and the trigger uncertainty with respect to the offline efficiency both serve directly as scale factors on the event yield.

The effect of various systematic uncertainties on data-driven background estimates based on either τ jet fake rates, embedding, or the inversion of event selection criteria, some of which are unique to the methods themselves, is explored in Section 5.

Table 2: Object-related systematic uncertainties.

Source of uncertainty	Uncertainty used in this analysis
Luminosity	$\pm 11\%$
E_T^{miss} resolution	Add or subtract object uncertainties into the E_T^{miss} , up to $\pm 20\%$
Jet energy resolution (JER)	$\approx \pm 14\%$, depending on η , see Reference [32]
Jet energy scale (JES)	$< \pm 10\%$ for $p_T > 15$ GeV and $ \eta < 4.5$, see Reference [33]
b-tagging efficiency	p_T dependent scale factor uncertainties, $\pm 10 - 12\%$, see Reference [27]
b-tagging mistag rate	Up to $\pm 26\%$, Reference [27] with further refinements
Tau identification efficiency	$\pm 6 - 12\%$, depending on p_T and number of associated tracks
Tau energy scale	$\pm 5\%$
Electron selection efficiency	$\pm 6 - 16\%$ as a function of p_T
Electron energy scale	$\pm 1\%$ for $ \eta < 1.4$, $\pm 3\%$ for $1.4 < \eta < 2.5$
Electron energy resolution	Sampling term $\pm 20\%$, a small constant term has a large variation with η
Muon selection efficiency	$\pm 1.2\%$ for $p_T < 20$ GeV and $\pm 0.4\%$ for $p_T > 20$ GeV
Muon momentum scale	η dependent scale offset in p_T , up to $\pm 3.5\%$
Muon momentum resolution	p_T and η dependent resolution smearing functions, $\leq \pm 10\%$
$\tau+E_T^{\text{miss}}$ trigger	$\pm 12\%$ with respect to offline, References [34, 35] with further refinements

4 Event selection

4.1 Event selection in the τ +jets final state

A topology of interest in the search for a charged Higgs boson decaying to $\tau\nu$ is

$$t\bar{t} \rightarrow [H^+ b] [W^- \bar{b}] \rightarrow [(\tau^+ \nu) b] [(j j) \bar{b}], \quad (1)$$

where both the W boson and the τ lepton decay hadronically; the neutrinos result in a large amount of E_T^{miss} . This topology has several advantages: the fact that the W boson can be reconstructed fully; the H^+ candidate mass can be reconstructed in the transverse plane (analogous to the transverse mass in

a W decay); and the larger branching fraction for W decaying into hadrons. However, there are also potentially serious challenges, such as the inherent presence of multi-jet final states which may make it difficult to distinguish this topology from the QCD multi-jet background.

The event selection is based on E_T^{miss} and τ -trigger selection, followed by the offline selection involving jets, b jet tagging, τ identification, and the selection of the highest- p_T $j\bar{j}b$ candidate (i.e., the reconstructed top-quark candidate from the decay $t \rightarrow Wb \rightarrow \text{jet-jet-}b$). The baseline selection is based on the objects and definitions in Section 3 and consists of the following requirements:

1. Event preselection:
 - (a) event-level cleaning cuts as described in Reference [20], with further refinements;
 - (b) E_T^{miss} plus τ -trigger;
 - (c) at least 4 jets with $p_T > 20$ GeV and $|\eta| < 4.9$.
2. Exactly one τ jet candidate with $p_T > 20$ GeV.
3. Events with any identified electrons or muons with $p_T > 10$ GeV are vetoed.
4. $E_T^{\text{miss}} > 20$ GeV.
5. $E_T^{\text{miss}} / \sqrt{\Sigma E_T} > 3 \text{ GeV}^{1/2}$.
6. At least one b -tagged jet.
7. The $j\bar{j}b$ system candidate with the highest $p_T^{j\bar{j}b}$ value must satisfy $m(j\bar{j}b) \in [120, 240]$ GeV.

The final discriminating variable is the $\tau + E_T^{\text{miss}}$ transverse mass, m_T , which in the case of most backgrounds corresponds to the transverse W mass and in the case of the signal hypothesis corresponds to the transverse H^+ mass. Explicitly, m_T is defined as

$$m_T = \sqrt{2p_T^\tau E_T^{\text{miss}}(1 - \cos \Delta\phi)}, \quad (2)$$

where $\Delta\phi$ is the angle between the τ jet and the missing momentum in the transverse plane. Using this selection, a total of 33 events are observed in 36 pb^{-1} of data.

4.2 Event selection in the τ +lepton final state

In this channel, the event signature is based on the leptonically decaying W boson ($l = e, \mu$, or τ with e/μ decays) and the presence of a hadronically-decaying τ . Neutrinos in the event result in a large amount of E_T^{miss}

$$t\bar{t} \rightarrow [H^+ b] [W^- \bar{b}] \rightarrow [(\tau^+ \nu) b] [(l^- \bar{\nu}) \bar{b}]. \quad (3)$$

The signal can manifest itself as an excess of τ leptons above the irreducible Standard Model background of $t\bar{t}$ production. Since at least three neutrinos are expected to be present in the final state, a full event reconstruction is not possible. The lepton originating from the W decay allows for the use of a highly efficient trigger.

The baseline event selection is built around an isolated lepton trigger requirement, missing transverse energy, tagged b jets, and a τ jet. It is based on the objects and definitions in Section 3 and consists of the following requirements:

1. Event preselection:
 - (a) event-level cleaning cuts as described in Reference [20], with further refinements;
 - (b) lepton trigger;
 - (c) exactly one trigger-matched isolated lepton with $p_T > 20$ GeV.
2. Exactly one τ jet with $p_T > 20$ GeV.

3. At least two jets with $p_T > 20$ GeV and $|\eta| < 4.9$.
4. At least one of the jets is b -tagged.
5. $\sum E_T > 200$ GeV.
6. Selected τ jet and lepton have opposite charge.
7. $E_T^{\text{miss}} > 60$ GeV.

Using this selection, a total of 11 events are observed in 37 pb^{-1} of data.

5 Data-driven background estimation

Events coming from production processes such as $t\bar{t}$, single top-quark, W +jets, Z +jets and QCD multi-jets make up the dominant background to charged Higgs boson searches at the LHC. The individual contributions from many of these backgrounds can be determined in a data-driven way. Events in which electrons, muons, or jets are misidentified as τ jets are predicted using methods based on fake rates. In this note, a fake rate is understood as the number of objects (e , μ or jet) being identified as a τ jet divided by all objects considered for τ identification (called τ jet candidates). Background events containing true τ jets are studied with the embedding method. The QCD multi-jet background is estimated in the τ +jets analysis using a data-driven control sample.

5.1 Events with electrons misidentified as τ jets

The τ identification has been optimized separately for a high QCD jet rejection, and for the rejection of electrons [26]. The probability that an electron is misidentified as a τ jet can be estimated from data.

5.1.1 Method

A technique to derive this fake rate from data is the so-called tag-and-probe method. The process $Z \rightarrow ee$ allows the selection of an unbiased and clean sample of electrons from data. While the tag electron is required to satisfy a tight electron selection, the other, if it is reconstructed as a τ jet candidate, is then used as the probe.

Only those probe τ jet candidates with exactly one associated track are considered as the rate of electrons faking 3-track τ jets is negligible compare to the 1-track case. The individual requirements for both the τ +jets and τ +lepton analyses are applied, this includes the electron veto and the overlap removal with electron candidates.

5.1.2 Results

The measured fake rates are shown in Figure 2. Within uncertainties, the fake rates modeled in Monte Carlo agree with those obtained from data.

5.1.3 Systematic uncertainties

Three main sources of systematic uncertainties on the electron-to- τ fake rate have been studied. The largest contribution originates from the background contamination with QCD jets (after the application of the electron veto on the probe object, QCD jets are enhanced with respect to electrons among the τ jet candidates) and gives an uncertainty of about 30%. The choice of the mass window size around the Z boson mass applied to the tag-and-probe objects introduces another uncertainty (13%). The uncertainty of the electron energy scale (via the cut on the tag electron energy) only gives a small contribution (2%). The total systematic uncertainty varies slightly with p_T and η and is estimated to be 33%.

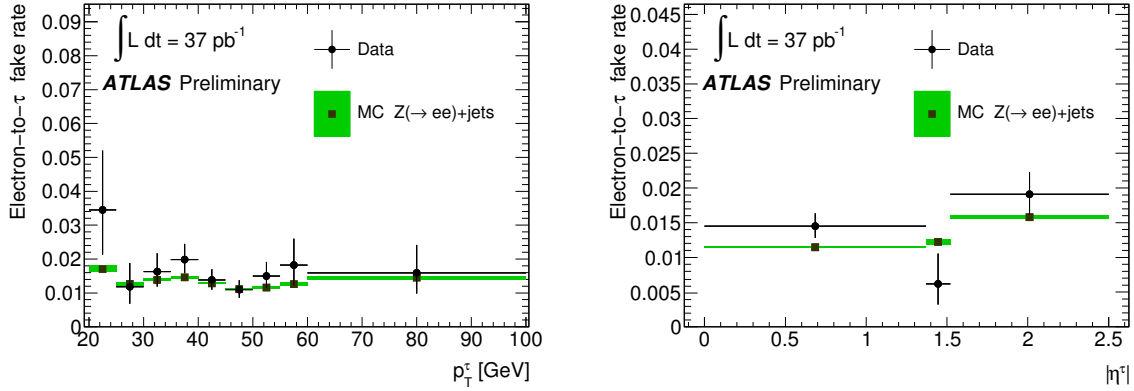


Figure 2: The fake rate for probe objects passing the τ identification, the electron veto, and overlap removal with reconstructed electrons is shown parametrized in p_T and $|\eta|$. The uncertainties indicated are statistical only.

5.1.4 Application to estimate the electron-to- τ fake background to the H^+ selections

The electron-to- τ fake background is estimated the following way: In simulated events, any true electron matched to a τ jet candidate is labeled as an identified τ jet and the event is given a weight equal to the probability given by the fake rate measured in this section, instead of performing the usual τ identification (i.e. the τ identification part is taken from data instead of simulation). All relevant quantities (E_T^{miss} , ΣE_T , E_T^{miss} significance, m_T , opposite-charge requirement) are then recalculated under the hypothesis that the electron is identified as a τ jet. The baseline selections of both the τ +jets and the τ +lepton channels (with the exception of the τ log-likelihood identification requirements) are then applied and the number of events surviving is counted (summing the weights of these events). The prediction using the fake rate derived from data and the expectation from Monte Carlo are shown in Table 3.

Table 3: Application of the fake rate obtained from $Z \rightarrow ee$ events. The numbers shown are the expected number of events after the baseline τ +lepton selection (normalized to 37 pb^{-1}), and after the baseline τ +jets selection (normalized to 36 pb^{-1}), for one-track τ jets. The predictions based on the fake rate measurement (the first uncertainty is statistical and the second is systematic), as well as the Monte Carlo prediction (statistical uncertainties only), are given.

Selection	Sample	Fake rate prediction [num. of events]	MC prediction [num. of events]
τ +jets	$t\bar{t}$	$1.08 \pm 0.01(\text{stat}) \pm 0.38(\text{syst})$	$1.50 \pm 0.09(\text{stat})$
τ +lepton	$t\bar{t}$	$0.65 \pm 0.01(\text{stat}) \pm 0.04(\text{syst})$	$0.79 \pm 0.08(\text{stat})$

5.2 Events with muons misidentified as τ jets

The muon-to- τ fake rate has been studied in a control sample of $Z \rightarrow \mu\mu$ events, in a similar manner as the electron-to- τ fake rate described in Section 5.1. The Monte Carlo description of the muon-to- τ fake rate is found to be consistent with that in data. Since the Monte Carlo expectation is that this background is 2-3 orders of magnitude smaller than even the uncertainties of other backgrounds, it is concluded that the background due to muons misidentified as τ jets is negligible.

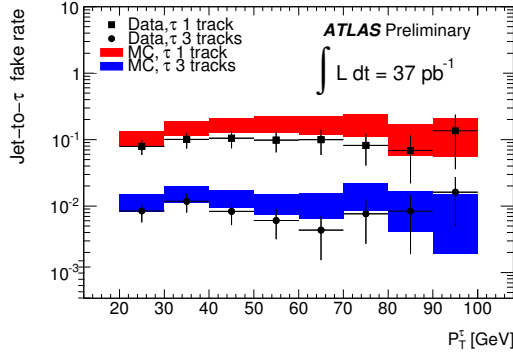


Figure 3: Jet-to- τ fake rates measured from γ +jet events for 1-track and 3-track τ jets. Statistical and systematic uncertainties are given for Monte Carlo, while the uncertainties shown for data are only statistical.

5.3 Events with jets misidentified as τ jets

A measurement of the probability of jets to be misidentified as τ jets is performed using γ +jet events selected from collision data. This particular control sample is selected as the jet in these events is dominantly quark-initiated (as opposed to QCD jets events, where jets are dominantly gluon-initiated) which is also the case for the background investigated in this section, i.e., $t\bar{t}$, single top-quark, and W +jets. The resulting fake rate is used to predict the part of these backgrounds which is due to jet-to- τ fakes, for both the τ +jets and τ +lepton analyses.

5.3.1 Method

For the measurement of the jet $\rightarrow\tau$ fake rate, events are required to pass a γ trigger. Identified γ s are required to be matched to the trigger object and pass a tight isolated photon selection. They must have $|\eta| < 2.5$ and a transverse momentum of at least 25 GeV. Events are selected which have one γ and a jet of $p_T > 20$ GeV separated by a ΔR of at least 0.7. The fake rate is binned in number of tracks associated to the τ jet candidate and in p_T . The object going into the denominator of the fake rate calculation is a τ jet candidate which must have $p_T > 20$ GeV, $|\eta| < 2.5$, 1 or 3 associated tracks, and pass lepton vetoes in order to reduce lepton fakes that would otherwise contaminate the fake measurement.

Objects going into the numerator of the fake rate calculation must pass the complete τ identification as described in Section 3. They must also have between 1 and 3 associated tracks, not be within ΔR of 0.4 of any e or μ passing the common object selection, and pass the cuts for reconstructed τ identification. Once measured, the fake rate can be applied to MC to test its ability to accurately measure the number of fakes and to predict fakes in data. The resulting fake rates are shown in Figure 3.

5.3.2 Systematic uncertainties

The systematic uncertainties considered are (the values depend slightly on p_T):

- Contamination of the control sample with true τ jets from $Z \rightarrow \tau\tau$ and $W \rightarrow \tau\nu$ (negligible).
- Contamination of the control sample with QCD multi-jet events. This is tested by investigating the effect of modifying the photon identification requirements on the measured fake rate, in particular loosening the photon isolation which increases the impurity from QCD jets in the control sample ($\approx 10\%$).

- Uncertainties of the control samples selection. This is tested by varying the selection cuts, and by splitting the control sample into a part which fulfils even tighter requirements and one which does not, and then taking the variation of the fake rate due to these changes as the uncertainty ($\approx 15\%$).
- Correlations between the tag and probe objects. This is evaluated by changing the selection requirements for the tag object and studying the impact on the fake rate ($\approx 3\%$).

The total systematic uncertainty is about 20% in the p_T range of interest. The statistical uncertainty on the fake rate is a systematic uncertainty for any application of the fake rate, and grows rapidly with p_T , as shown in Figure 3.

5.3.3 Application to estimate the fake-jets background to the H^+ selections

In simulated events, any jet matched to a τ jet candidate as defined by the denominator requirements of the fake rate detailed in Section 5.3.1 is labeled as a τ jet (instead of performing the offline hadronic τ identification), and given a weight equal to the calculated fake rate value. In order to avoid double-counting, the jet that corresponds to this hadronic τ is removed from the event, affecting the number of reconstructed jets, ΣE_T of the event, E_T^{miss} , the E_T^{miss} significance, the number of b -tagged jets, and the top quark reconstruction. For all events which pass the event selection after taking this into consideration, the weight is summed. The number of events predicted for collision data, together with a comparison to the prediction using Monte Carlo truth information, is shown in Table 4 both for the τ +jets and the τ +lepton baseline selection (see Section 4). Within uncertainties, the predictions agree well.

Table 4: Application of the fake rate obtained from γ +jet events. The numbers shown are the expected number of events in collision data after the baseline τ +lepton selection (normalized to 37 pb^{-1}), and after the baseline τ +jets selection (normalized to 36 pb^{-1}). The predictions based on the fake rate measurement (statistical and systematic uncertainties), as well as the Monte Carlo prediction (statistical uncertainties), are given.

Selection	Sample	Fake rate prediction [num. of events]	MC prediction [num. of events]
τ +jets	$t\bar{t}$	$1.7 \pm 0.2 \text{ (stat)} \pm 0.3\text{(syst)}$	$1.9 \pm 0.2 \text{ (stat)}$
τ +lepton	$t\bar{t}$	$6.7 \pm 1.0 \text{ (stat)} \pm 1.4\text{(syst)}$	$6.0 \pm 0.2 \text{ (stat)}$
τ +lepton	W +jets	$0.9 \pm 0.1 \text{ (stat)} \pm 0.2\text{(syst)}$	$0.6 \pm 0.3 \text{ (stat)}$
τ +lepton	Single top	$0.16 \pm 0.02\text{(stat)} \pm 0.03\text{(syst)}$	$0.12 \pm 0.02\text{(stat)}$
τ +lepton	Z +jets	$0.15 \pm 0.02\text{(stat)} \pm 0.03\text{(syst)}$	$0.3 \pm 0.2 \text{ (stat)}$

5.4 QCD Background Estimate

5.4.1 Method

The following method is used to estimate the QCD jets background to the τ +jets analysis. In order to model the QCD background from data, an orthogonal event selection is defined which is identical to the complete τ +jets event selection, except for requiring a looser τ identification while rejecting events using the tighter τ identification used in the baseline selection.

This selection, referred to as “inverted selection” in this section, is applied to data and the shape of the E_T^{miss} distribution is used as a model for the QCD background (after subtracting the contribution from the background expectation from simulation for non-QCD processes). Then, a fit is performed to the E_T^{miss} distribution in data resulting from the baseline τ +jets selection (after all cuts), using two shapes:

the model extracted for the QCD background, and the sum of non-QCD processes (dominated by $t\bar{t}$, W +jets) for which the shape and the relative normalization is taken from MC simulation.

The fit floats the overall normalization (to the one in data) and the QCD fraction. The underlying assumption is that the shape of the E_T^{miss} distribution for QCD is the same for the baseline and the inverted selection. This is shown in Figure 4 where the two distributions are compared for collision data. The comparison is done after selection cuts 1–3 as described in Section 4.1 have been applied, as this ensures that the distributions are QCD-dominated. In spite of the QCD-dominance, the contribution of events with true E_T^{miss} , like $t\bar{t}$ and W +jets, is still significant in the tail of the distribution. For this reason, their expectation from simulation has been subtracted. Only a very small number of QCD events is observed for $E_T^{\text{miss}} > 100$ GeV, as expected. The remaining differences are within statistical uncertainties.

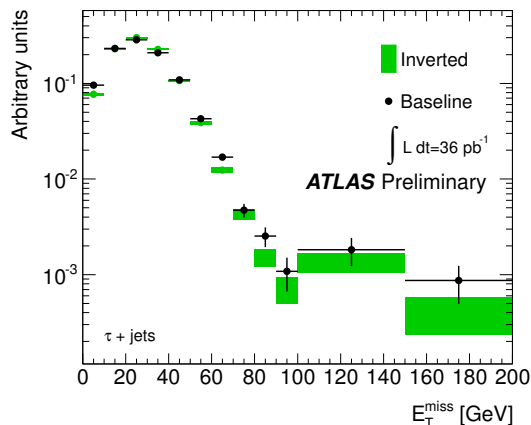


Figure 4: Distribution of E_T^{miss} for data, after subtracting the expectation from $t\bar{t}$, W +jets and single top-quark simulation. The comparison is done after selection cuts 1–3 as described in Section 4.1 have been applied, as this ensures that the distributions are QCD-dominated. The error bars show the size of the data statistical uncertainties.

5.4.2 Results

The result of the fit is shown in Figure 5. The QCD fraction is estimated to be $(54 \pm 19)\%$ for the 1-track τ case. There are not enough 3-track events in data after the baseline selection, thus no separate fit is performed and instead, both the 1- and 3-track cases are fitted simultaneously. The QCD fraction is estimated to be $(57 \pm 19)\%$.

5.4.3 Systematic uncertainties

The dominant systematic uncertainties are:

- Using $t\bar{t}$ and W +jets shape and relative normalization from Monte Carlo, dominated by uncertainties on the $t\bar{t}$ cross section: 15%.
- E_T^{miss} shape difference in signal and control region: 5%.

The contamination in the control region from backgrounds that were not considered is negligible. Currently, the systematic uncertainty is dominated by the statistical uncertainty of the limited size of the data set on which the fit is applied, amounting to 33%. However, this component will naturally decrease as the collected integrated luminosity increases. Uncertainties related to the cross sections and shapes of other backgrounds will also decrease once they are measured with high accuracy at the LHC.

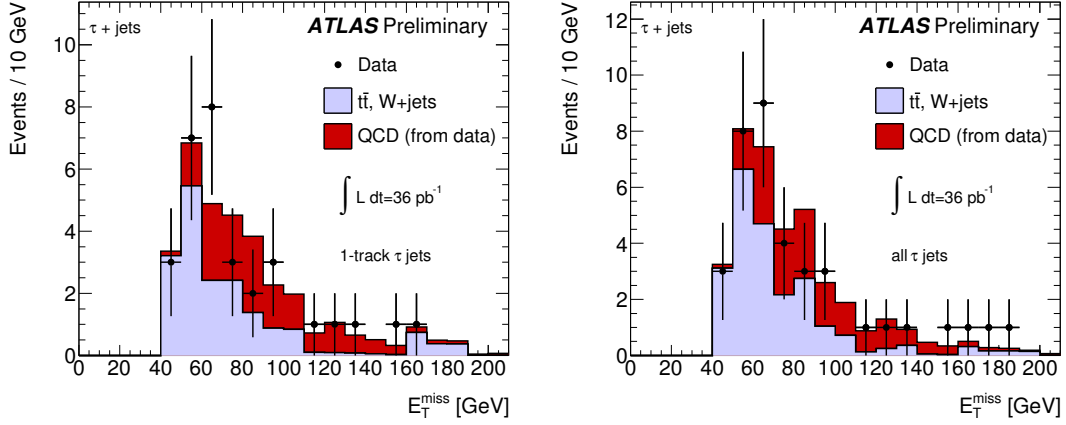


Figure 5: Fit to E_T^{miss} after all selection cuts using two shapes: one for the QCD model and one for $t\bar{t}$ and W +jets (all other backgrounds are negligible and not shown). Left: 1-track τ jets. Right: 1-track and 3-track τ jets together. The error bars show the size of the data statistical uncertainties.

5.4.4 Application to estimate the QCD background to the τ +jets selection

The estimated QCD jets contribution to the final m_T distribution is shown in Figure 6. All other backgrounds have W bosons in the final state and their distributions drop off around the W boson mass, as expected. Such behaviour is neither expected nor observed for the QCD jets background as the sources of both the τ jet and E_T^{miss} are fakes and the resulting shapes are thus not steered by a specific physics process but by instrumental effects. To probe the region with large m_T , in which a potential H^+ signal resides, it is thus important to suppress the QCD jets background as much as possible. This can be done with a tighter τ identification and harder E_T^{miss} requirements once a larger data set becomes available. The estimated QCD jets contribution after all cuts is $18.8 \pm 6.2(\text{stat}) \pm 3.0(\text{syst})$ events.

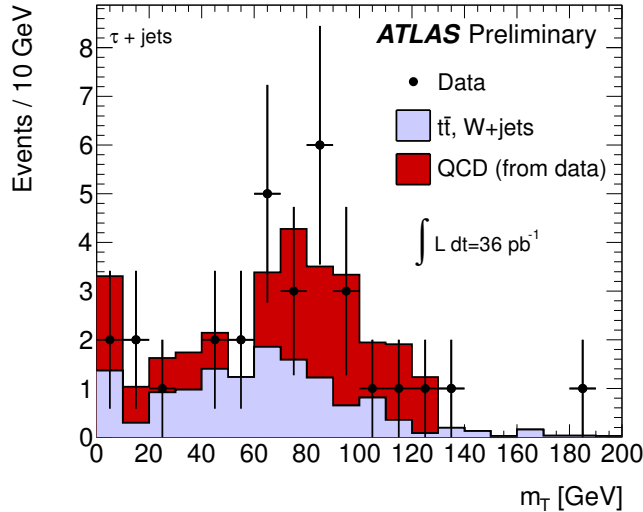


Figure 6: Estimated QCD jets contribution to the m_T distribution after all cuts of the baseline τ +jets selection. The data is shown, together with the fit for $t\bar{t}$ and W +jets contributions, where the shapes have been taken from simulation. The error bars show the size of the data statistical uncertainties.

5.5 Embedding method

Embedding tools are used for estimating the background with true τ jets for the τ +jets analysis. The method consists of collecting a control sample containing $t\bar{t}$, single top-quark production and W +jet events with muons, replacing the detector signature of the muon with a simulated τ lepton, re-reconstructing the new hybrid event, and then using these events instead of simulation for background estimation. The advantage is that the whole event (except for the τ jet) is taken directly from data, including the underlying event and pile-up, b -quark jets and light-quark jets.

5.5.1 Method

Control sample collection. To select the μ +jets control sample from data, the following event selection is used, based on the objects and definitions in Section 3:

- Event-level cleaning cuts.
- Event passed a trigger requiring the presence of a muon candidate.
- Exactly one isolated muon with $p_T > 20$ GeV.
- No electron with $p_T > 20$ GeV.
- At least three jets with $p_T > 20$ GeV.
- At least one of the jets is tagged as b jet.
- A reconstructed invariant mass of two jets with $p_T > 35$ GeV in a mass window of 20 GeV around the nominal W boson mass.
- Missing transverse energy $E_T^{\text{miss}} > 30$ GeV.
- Scalar sum of the energy in the calorimeter $\Sigma E_T > 200$ GeV.

The expected and observed number of events are shown in Table 5 and agree well.

Table 5: Expected (from simulation) and observed number of events in the embedding control sample. Statistical uncertainties only.

	Expected					Observed
	$t\bar{t}$	Single top-quark	W +jets	QCD	Sum	Data
Events	171.2 ± 1.4	11.3 ± 0.3	16.8 ± 2.1	12.4 ± 3.2	212 ± 7	219

The impurity from backgrounds with muons produced in τ decays, and non-isolated muons (dominantly $b\bar{b}$ and $c\bar{c}$ events) is at the level of 10% and biases the shape of embedded events as there is no physical correspondence to such embedded events. However, as is shown below, the bias is reduced as these events typically have a softer μ spectrum ($W \rightarrow \tau\nu \rightarrow \mu\nu\nu\nu$ as compared to $W \rightarrow \mu\nu$, and muons from B and D meson decays) and thus mostly contribute to the low-mass tail of the m_T distribution which is not considered.

Embedding step. After events have been selected, the actual embedding takes place. The muon in the event is selected, its vertex position and momentum are extracted. The momentum is then rescaled to account for the higher τ -lepton mass, and fed into TAUOLA to produce the τ -lepton decay products and generate final-state radiation. The result is propagated through the ATLAS detector simulation, followed by reconstruction.

In the next step, tracks and calorimeter cell depositions in the vicinity of the muon are replaced with those of the τ -lepton decay products—in other words, the simulated τ event is embedded in the collision data event. Then the reconstruction algorithms are re-run on this hybrid event, reconstructing τ jets, leptons, missing transverse energy, and other high-level physics objects.

5.5.2 Application to estimate the true- τ background to the τ +jets selection

The contribution of backgrounds with true τ jets to the final m_T distribution is estimated from this distribution for embedded events. The normalization is taken from collision data events in the region $30 < m_T < 70$ GeV, where both the QCD background contribution and the signal contamination are low. The following procedure is applied:

1. Obtain the m_T distribution after the τ +jets baseline selection from embedded events.
2. From collision data, count the number of events after applying the τ +jets selection in the m_T distribution between $30 < m_T < 70$ GeV (after subtracting the background from fake τ jets).
3. Using this number, normalize the m_T distribution from embedding using the ratio of events in collision data and embedded events in the region $30 < m_T < 70$ GeV.

Currently, the method is statistics-limited and thus the selection applied to the embedded events is loosened compared to that given in Section 4.1: no trigger requirement is applied to the embedded samples and the τ identification is replaced by matching a τ candidate to the true τ in the event. Requirements related to the second top quark $t \rightarrow bqq$ in the event are dropped as they are not expected to influence the m_T shape, namely the reconstruction of this hadronic top quark in a mass window and the requirement of having at least four jets in the event (loosened to three). In Figure 7, it is shown that the impact of this loosened selection on the m_T shape, as compared to the same distribution for the baseline selection, can be taken into account by a systematic uncertainty of 20%, which is less than the statistical uncertainty associated to the set of embedding events. Figure 7 also shows the m_T distribution obtained from embedded simulation events (left) and data (right).

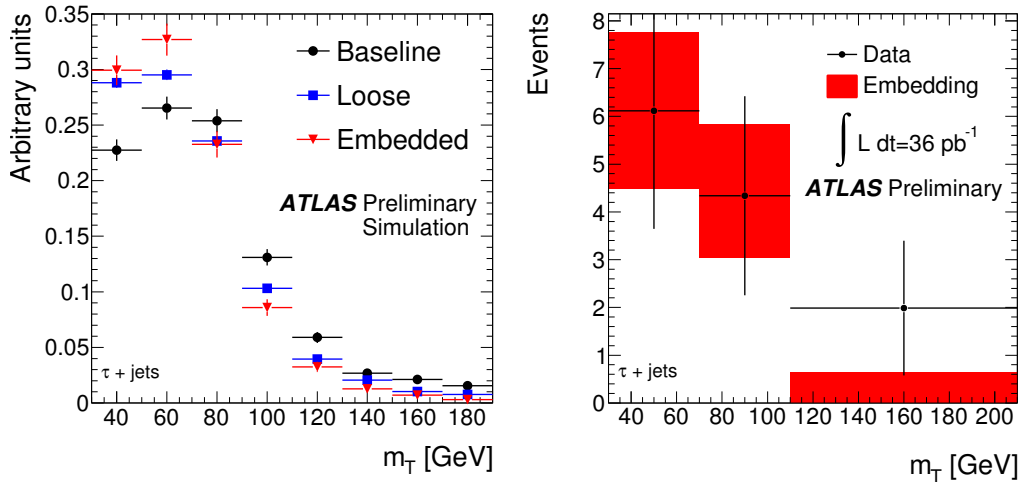


Figure 7: Left: Comparison of the m_T shape in simulation for selections which have been loosened with respect to the τ +jets selection. Shown is the shape for the full selection (Baseline), and when removing the trigger, the τ identification requirement (replaced by matching a τ candidate to a true τ), not using the top quark reconstruction requirement and only requiring a minimum of three instead of four jets (Loose). Additionally, this loosened selection is also applied to an embedded $t\bar{t}$ simulation sample (Embedded). Statistical uncertainties are shown. Right: Comparison of the m_T shape embedded versus collision data after subtracting the contributions from fake τ , as estimated in previous sections, from the data. The comparison is done after the τ +jets event selection described in Section 4.1 and after normalizing the embedding distribution to the data distribution in the range $30 < m_T < 70$ GeV. Statistical and systematic uncertainties are shown.

As can be seen, the background estimate is currently limited by the statistical uncertainty due to the limited number of events in the $t\bar{t}$ control sample. In the range $70 < m_T < 210$ GeV, $4.7 \pm 1.3^{+1.4}_{-1.1}$ background events with true τ jets are expected and 6.3 ± 2.5 are observed in excess of the background predicted by the fake rate methods and the QCD fit. Within large statistical uncertainties, the background prediction and data agree well.

5.5.3 Systematic uncertainties

The following systematic uncertainties are associated to the background prediction:

- Differences in shapes of distributions between events with an embedded τ compared to a reference; considering Figure 7, the uncertainty is estimated to be $\pm 10\%$. This includes the impact of the control sample selection (e.g. the muon trigger efficiency, the η dependence of the offline muon selection) and the contamination from non-isolated muons and muons from τ decays.
- Difference in m_T shape due to the loosening of the selection with respect to the baseline selection, as shown in Figure 7: -20% .
- Uncertainties in the subtraction of fake- τ backgrounds from data: $\pm 20\%$.

An additional statistical uncertainty of about 30% is larger than the systematic uncertainties.

6 Summary of data-driven estimates

The results of the data-driven methods introduced and explained in Section 5 are summarized for each of the τ +jets and τ +lepton final state analyses, and compared to collision data.

6.1 τ +jets channel

The results of the data-driven methods in estimating the contributions of the various categories of backgrounds after the baseline selection are summarized in Table 6 and the m_T distribution of the remaining events is shown in Figure 8. The number of events with true τ jets has been estimated with the embedding method, the jet $\rightarrow \tau$ fakes with γ +jet control samples, the $e \rightarrow \tau$ fakes with $Z \rightarrow ee$ control samples and the QCD contribution by taking its shape from a sideband region and fitting it to the data. Both the total number of events, and the number of events with $m_T > 70$ GeV is given. This allows for a better comparison of data and expectation as the estimate from the embedding method is fitted to data in the range $30 < m_T < 70$ GeV. The uncertainties are still large, but a good agreement between estimated and observed events is seen.

Table 6: Expected number of events from data-driven estimates and as observed in data for the τ +jets channel.

	Expected					Observed
	True τ jets	Jet $\rightarrow \tau$ fakes	$e \rightarrow \tau$ fakes	QCD	Sum	Data
All events	$10.8 \pm 3.1^{+3.2}_{-2.4}$	$1.7 \pm 0.2 \pm 0.3$	$1.1 \pm 0.0 \pm 0.4$	$18.8 \pm 6.2 \pm 3.0$	$32 \pm 9 \pm 7$	33
$m_T > 70$ GeV	$4.7 \pm 1.3^{+1.4}_{-1.1}$	$1.2 \pm 0.2 \pm 0.2$	$0.7 \pm 0.0 \pm 0.3$	$11.3 \pm 3.7 \pm 1.7$	$18 \pm 5 \pm 4$	17

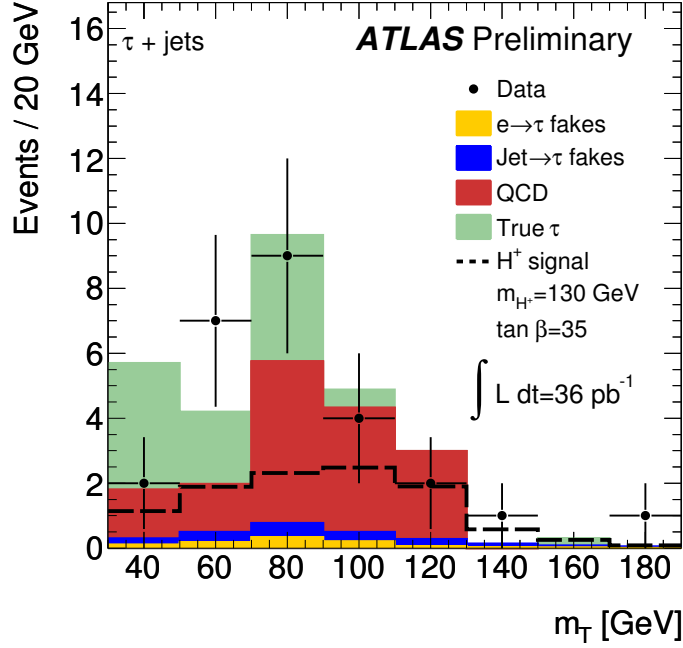


Figure 8: The $\tau + E_T^{\text{miss}}$ transverse mass distribution at the end of the event selection for the τ +jets channel comparing the observation in collision data, and the estimates from data-driven methods. The error bars show the size of the data statistical uncertainties. The distribution of the H^+ signal is given for a reference point in parameter space corresponding to $\text{BR}(t \rightarrow bH^+) \approx 6\%$, thus the SM-like $t\bar{t}$ background and its contribution to the $e \rightarrow \tau$ and jet $\rightarrow \tau$ fake background would be reduced correspondingly.

6.2 τ +lepton channel

For the second final state under investigation, the results are summarized in Table 7, and the E_T^{miss} distribution of the remaining events is shown in Figure 9. The number of events with true τ jets is taken from simulation, while the contribution of jet $\rightarrow \tau$ fakes and $e \rightarrow \tau$ fakes is estimated using γ +jet and $Z \rightarrow ee$ control samples. In this channel, the QCD jets background is negligible mostly due to the lepton and the E_T^{miss} requirements. A good agreement between the estimated and the observed value is seen.

Table 7: Expected number of events from data-driven estimates and as observed in data for the τ +lepton channel. The number of events with true τ jets is taken from simulation.

	Expected			Sum	Observed
	True τ jets	Jet $\rightarrow \tau$ fakes	$e \rightarrow \tau$ fakes		Data
Events	$6.9 \pm 0.3 \pm 1.4$	$7.9 \pm 1.1 \pm 1.6$	$0.65 \pm 0.01 \pm 0.04$	$15.5 \pm 1.4 \pm 3.0$	11

7 Conclusions

Data-driven methods are used in 37 pb^{-1} of $\sqrt{s} = 7 \text{ TeV}$ data to estimate the number of events characterized by the presence of a τ jet, E_T^{miss} , b jets, and a hadronically or leptonically decaying W boson. The events are predominantly expected to come from $t\bar{t}$, W or Z +jets, single top-quark, and QCD events and represent backgrounds to charged Higgs boson searches. Predictions of $32 \pm 9(\text{stat}) \pm 7(\text{syst})$

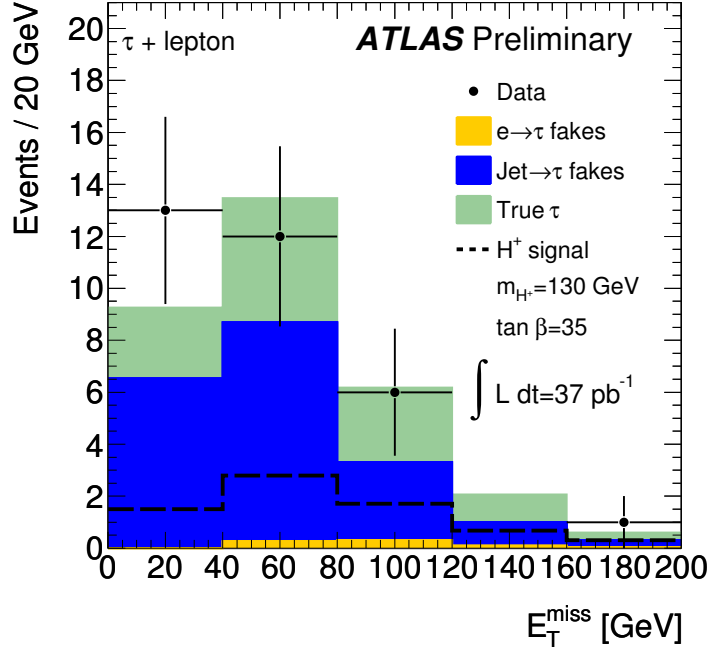


Figure 9: The E_T^{miss} distribution at the end of the event selection for the τ +lepton channel comparing the observation in collision data, and the estimates from data-driven methods. The error bars show the size of the data statistical uncertainties. The distribution of the H^+ signal is given for a reference point in parameter space corresponding to $\text{BR}(t \rightarrow bH^+) \approx 6\%$, thus the SM-like $t\bar{t}$ background and its contribution to the $e \rightarrow \tau$ and jet $\rightarrow \tau$ fake background would be reduced correspondingly.

($18 \pm 5(\text{stat}) \pm 4(\text{syst})$ with $m_T > 70$ GeV) and $15.5 \pm 1.4(\text{stat}) \pm 3.0(\text{syst})$ events are achieved in the τ +jets and τ +lepton channels, respectively. The observation of 33 events (17 with $m_T > 70$ GeV) in the τ +jets channel and 11 events in the τ +lepton channel is consistent with expectations based on these data-driven background estimation methods. The study presented here serves as a foundation for future charged Higgs boson searches in the hadronically-decaying τ final state using larger amounts of integrated luminosity.

References

- [1] J. F. Gunion, H. E. Haber, G. L. Kane, and S. Dawson, *The Higgs Hunter's Guide*. Addison-Wesley, 1990. 94/205 -Lacker.
- [2] J. F. Gunion, H. E. Haber, G. L. Kane, and S. Dawson, *Errata for "The Higgs Hunter's Guide"*, hep-ph/9302272.
- [3] A. Djouadi, *The Anatomy of electro-weak symmetry breaking. II. The Higgs bosons in the minimal supersymmetric model*, Phys. Rept. **459** (2008) 1–241, arXiv:hep-ph/0503173.
- [4] ATLAS Collaboration, G. Aad et al., *Expected Performance of the ATLAS Experiment - Detector, Trigger and Physics*, CERN-OPEN-2008-020, arXiv:0901.0512 [hep-ex].
- [5] S. Frixione and B. R. Webber, *Matching NLO QCD computations and parton shower simulations*, JHEP **06** (2002) 029, arXiv:hep-ph/0204244.

- [6] G. Corcella, I. Knowles, G. Marchesini, S. Moretti, K. Odagiri, et al., *HERWIG 6: An Event generator for hadron emission reactions with interfering gluons (including supersymmetric processes)*, JHEP **0101** (2001) 010, arXiv:hep-ph/0011363 [hep-ph].
- [7] J. Butterworth, J. R. Forshaw, and M. Seymour, *Multiparton interactions in photoproduction at HERA*, Z.Phys. **C72** (1996) 637–646, arXiv:hep-ph/9601371 [hep-ph].
- [8] S. Frixione, E. Laenen, P. Motylinski, and B. R. Webber, *Single-top production in MC@NLO*, JHEP **03** (2006) 092, arXiv:hep-ph/0512250.
- [9] ATLAS Collaboration, G. Aad et al., *Measurement of the top quark-pair production cross section with ATLAS in pp collisions at $\sqrt{s} = 7$ TeV*, arXiv:1012.1792 [hep-ex].
- [10] U. Langenfeld, S. Moch, and P. Uwer, *New results for $t\bar{t}$ production at hadron colliders*, arXiv:0907.2527 [hep-ph].
- [11] M. L. Mangano, M. Moretti, F. Piccinini, R. Pittau, and A. D. Polosa, *ALPGEN, a generator for hard multiparton processes in hadronic collisions*, JHEP **07** (2003) 001, arXiv:hep-ph/0206293.
- [12] J. Alwall, S. Hoche, F. Krauss, N. Lavesson, L. Lonnblad, et al., *Comparative study of various algorithms for the merging of parton showers and matrix elements in hadronic collisions*, Eur.Phys.J. **C53** (2008) 473–500, arXiv:0706.2569 [hep-ph].
- [13] T. Sjostrand, S. Mrenna, and P. Z. Skands, *PYTHIA 6.4 Physics and Manual*, JHEP **05** (2006) 026, arXiv:hep-ph/0603175.
- [14] Z. Was and P. Golonka, *TAUOLA as tau Monte Carlo for future applications*, Nucl.Phys.Proc.Suppl. **144** (2005) 88–94, arXiv:hep-ph/0411377 [hep-ph].
- [15] E. Barberio, B. van Eijk, and Z. Was, *PHOTOS: A universal Monte Carlo for QED radiative corrections in decays*, Comput. Phys. Commun. **66** (1991) 115–128.
- [16] ATLAS Collaboration, G. Aad et al., *Charged particle multiplicities in pp interactions at $\sqrt{s} = 0.9$ and 7 TeV in a diffractive limited phase-space measured with the ATLAS detector at the LHC and new PYTHIA6 tune*, ATLAS-CONF-2010-031 (2010) .
- [17] ATLAS Collaboration, G. Aad et al., *First tuning of HERWIG/JIMMY to ATLAS data*, ATL-PHYS-PUB-2010-014 (2010) .
- [18] ATLAS Collaboration, G. Aad et al., *The ATLAS Simulation Infrastructure*, Eur.Phys.J. **C70** (2010) 823–874, arXiv:1005.4568 [physics.ins-det].
- [19] GEANT4 Collaboration, S. Agostinelli et al., *GEANT4: A simulation toolkit*, Nucl. Instrum. Meth. **A506** (2003) 250–303.
- [20] ATLAS Collaboration, *Data-Quality Requirements and Event Cleaning for Jets and Missing Transverse Energy Reconstruction with the ATLAS Detector in Proton-Proton Collisions at a Center-of-Mass Energy of $\sqrt{s} = 7$ TeV*, ATLAS-CONF-2010-038 (2010) .
- [21] M. Cacciari, G. P. Salam, and G. Soyez, *The Anti- $k(t)$ jet clustering algorithm*, JHEP **0804** (2008) 063, arXiv:0802.1189 [hep-ph].
- [22] M. Cacciari and G. P. Salam, *Dispelling the N^3 myth for the $k(t)$ jet-finder*, Phys.Lett. **B641** (2006) 57–61, arXiv:hep-ph/0512210 [hep-ph].

- [23] W. Lampl et al., *Calorimeter clustering algorithms: Description and performance*, ATL-LARG-PUB-2008-002 (2010) .
- [24] ATLAS Collaboration, *Properties of Jets and Inputs to Jet Reconstruction and Calibration with the ATLAS Detector Using Proton-Proton Collisions at $\sqrt{s} = 7$ TeV*, ATLAS-CONF-2010-053 (2010) .
- [25] ATLAS Collaboration, *Jet energy scale and its systematic uncertainty in proton-proton collisions at $\sqrt{s} = 7$ TeV in ATLAS 2010 data*, ATLAS-CONF-2011-032 (2011) .
- [26] ATLAS Collaboration, *Tau Reconstruction and Identification Performance in ATLAS*, ATLAS-CONF-2010-086 (2010) .
- [27] ATLAS Collaboration, *Calibrating the b-Tag Efficiency and Mistag Rate of the SV0 b-Tagging Algorithm in 3/pb of Data with the ATLAS Detector*, ATLAS-CONF-2010-099 (2010) .
- [28] ATLAS Collaboration, *Electron and photon reconstruction and identification in ATLAS: expected performance at high energy and results at $\sqrt{s} = 900$ GeV*, ATLAS-CONF-2010-005 (2010) .
- [29] ATLAS Collaboration, *Muon Reconstruction Performance*, ATLAS-CONF-2010-064 (2010) .
- [30] ATLAS Collaboration, *Performance of the Missing Transverse Energy Reconstruction and Calibration in Proton-Proton Collisions at a Center-of-Mass Energy of $\sqrt{s} = 7$ TeV with the ATLAS Detector*, ATLAS-CONF-2010-057 (2010) .
- [31] ATLAS Collaboration, *Observation of $W \rightarrow \tau\nu_\tau$ Decays with the ATLAS Experiment*, ATLAS-CONF-2010-097 (2010) .
- [32] ATLAS Collaboration, *Jet Energy Resolution and Selection Efficiency Relative to Track Jets from In-situ Techniques with the ATLAS Detector using Proton-Proton Collisions at a Center of Mass Energy $\sqrt{s} = 7$ TeV*, ATL-CONF-2010-054 (2010) .
- [33] ATLAS Collaboration, *Jet energy scale and its systematic uncertainty for jets produced in proton-proton collisions at $\sqrt{s} = 7$ TeV and measured with the ATLAS detector*, ATL-CONF-2010-056 (2010) .
- [34] P. H. Beauchemin, *Performance of the ATLAS missing ET trigger with first $\sqrt{s} = 7$ TeV data*, ATL-DAQ-PROC-2010-024 (2010) .
- [35] ATLAS Collaboration, *Performance of the ATLAS tau trigger in p-p collisions at $\sqrt{s} = 7$ TeV*, ATLAS-CONF-2010-090 (2010) .